Sensors and Actuators B 183 (2013) 319–331

Contents lists available at SciVerse ScienceDirect

Sensors and Actuators B: Chemical

journal homepage: www.elsevier.com/locate/snb

Long-period fiber grating using the finite element method and eigenmode expansion method

Yue-Jing He*

Department of Electronic Engineering, National Chin-Yi University of Technology, Taichung 41170, Taiwan

ARTICLE INFO

Article history:
Received 22 January 2013
Received in revised form 30 March 2013
Accepted 7 April 2013
Available online 13 April 2013

Keywords:
Long period fiber grating
Finite element method
Eigenmode expansion method
Optical sensors
Optical communication component

ABSTRACT

Previous studies of long-period fiber grating (LPG) have commonly employed the traditional coupled-mode theory. In this study, however, we propose a visualized, graphical, and simplified numerical simulation method that incorporates the finite element method and eigenmode expansion method. The FEM was employed to solve the existing guided modes in the fiber structure, and the eigenmode expansion method was employed to calculate the power transmissions of the guided modes in the fiber structure. This study provides a detailed explanation of how the periodic structure of optical LPG renders this method significantly superior compared to other numerical methods, such as the finite-difference time-domain method and the beam propagation method. In other words, of all numerical simulation methods that focus on large-scale periodic components, only the method proposed in this study possesses 3D design and analysis capabilities. Additionally, a comparison between the period scan diagram of LPG and the final spectrum diagram showed that the two possessed a certain inverse relationship in the periods or wavelengths of coupling. Therefore, before conducting time-consuming calculations of the fiber grating spectra, this characteristic can be considered to predict the final spectrum. By combining these two numerical simulation methods and adopting a rigorous, simple, and complete design process, this study provides a graphical and simple simulation technique to reduce the required learning time and professional threshold for research and applications of LPG.

1. Introduction

Long-period fiber grating (LPG) written periodically into the core layer of a photosensitive optical fiber using ultraviolet light can couple the power among copropagating modes. Coupling between the core mode HE_{11} and cladding modes has been employed extensively for band rejection filters, gain flatteners, and dispersion compensators [1–3]. For a given azimuthal number l, several hundred cladding modes at near-infrared wavelength typically exist in a traditional communication fiber. According to the fundamental properties of modes, the higher the order of the cladding mode, the more the field can be extended. Obviously, a high-order cladding mode is more sensitive to environmental variations compared to a low-order mode. Therefore, various sensors based on high-order cladding modes have been proposed in recent years [4–7]. Long-period fiber grating (LPG) can also function as optical add-drop multiplexer (OADM) components [8,9] and optical fiber surface plasmon resonance sensors [10,11].

To date, the traditional coupled-mode theory is among the most widely used techniques in studies on the characteristics and applications of LPG. For novice researchers in the field of LPG, learning this theory is essential to understand all LPG-related physical concepts. The traditional coupled-mode theory plays a crucial role in understanding LPG-related properties. Below we use three brief points to demonstrate how the traditional coupled-mode theory is employed for conducting LPG analysis and design.

1.1. The definition of fiber structures and the solution for guided modes

The geometric structure of a normal optical fiber comprises three layers, that is, the core layer, the cladding layer, and the surrounding layer. The parameters of the layers are $a_1 = 2.5\ \mu m$, $a_2 = 62.5\ \mu m$, $n_1 = 1.458$, $n_2 = 1.45$, and $n_3 = 1$, as shown in Fig. 1. Notably, the ideal radius of the surrounding layer should be infinite. After the geometric structure of the fiber's X–Y plane is determined, the Maxwell equations are applied with the boundary conditions to derive the dispersion relation equations. Subsequently, by solving the dispersion relation equations, all guided modes in the structure can be obtained and each guided mode has a corresponding

* Tel.: +886 423924505; fax: +886 423926610.
E-mail address: yuejing@ncut.edu.tw

0925-4005/$ – see front matter © 2013 Elsevier B.V. All rights reserved.
http://dx.doi.org/10.1016/j.snb.2013.04.013

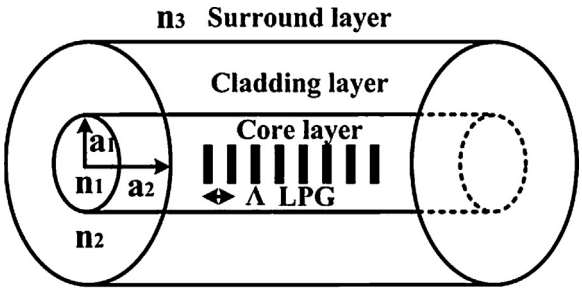

Fig. 1. The geometric structure and parameters of a typical optical fiber and LPG.

effective refractive index (n_{eff}^{ν}) [12,13]. From a strictly mathematic perspective, a mode is the resolution of a differential equation that fulfills a certain boundary condition. Unless specifically noted, we only analyze a single-mode communication fiber. In other words, we acquired one core mode (n_{eff}^{core}; $n_2 < n_{eff}^{core} < n_1$) and approximately infinite cladding modes ($n_{eff}^{cladding}$; $n_3 < n_{eff}^{cladding} < n_2$).

1.2. The definition of the fiber grating mathematical model and an explanation of the coupled-mode equation

Regarding the production of LPG, we first select single-mode optical fibers that use photosensitive materials in the core layer. Then, we use ultraviolet light to irradiate amplitude masks that possess certain periods to allow their power to form constructive and destructive interferences on the single-mode optical fibers, thereby altering the refractive index of the core layer. The mathematical model of uniform fiber grating is as follows:

$$n_1(z) = n_1 + \delta n\left[1 + \cos\left(\frac{2\pi}{\Lambda}z\right)\right]. \tag{1}$$

Here, δn is the peak-induced index change, and Λ is the period of the long-period fiber grating. From a mathematical perspective, before the emergence of fiber grating, the modes existing in fiber waveguides were orthogonal. That is, during the entire transmission process, the power between modes could not be interchanged or coupled. However, when LPGs were programmed into the core layer, power interference effects between the modes occurred. Appropriate design of the LPG period Λ can disrupt the orthogonality of the original model to thereby achieve the power coupling phenomenon. In a $\delta n \ll n_1$ condition, the mode coupling mathematical model can be represented as follows [10]:

$$\frac{dA_\mu}{dz} = iA_\nu K_{\nu-\mu}\exp[i(\beta_\nu - \beta_\mu)z] \tag{2}$$

in which

$$K_{\nu-\mu} = \frac{w}{2}\frac{\Delta\varepsilon\int_{A\infty}(E_r^\nu E_r^\mu + E_\varphi^\nu E_\varphi^\mu)dA - ((\Delta\varepsilon)/(\Delta\varepsilon+\varepsilon))\int_{A\infty}(E_z^\nu E_z^\mu)dA}{\int_0^{2\pi}\int_0^\infty(E_r^\mu H_\varphi^\mu - E_\varphi^\mu H_r^\mu)dA} \tag{3}$$

where A_μ and A_ν represent the amplitude of any guiding mode in the fiber, β_μ and β_ν represent the propagation constants of any guiding mode in the fiber, $K_{\nu-\mu}$ is the coupling coefficients between mode ν and mode μ, $\Delta\varepsilon$ represents the dielectric constant variation created by the LPG in the core layer, and w represents the angular frequency.

1.3. The definition of the bar and cross transmission power of the spectrum

To analyze the properties of the LPG spectrum, we defined the mathematical formula of the bar transmission power and cross transmission power as follows:

$$t_= = \frac{\left|R(z)\right|^2}{\left|R(0)\right|^2}, \tag{4}$$

$$t_\times = \frac{\left|S(z)\right|^2}{\left|R(0)\right|^2}. \tag{5}$$

Briefly, the bar transmission power is the power ratio of incident mode HE_{11} after transmission to distance (z) to its power at incidence ($z=0$). By contrast, if the power of incident mode HE_{11} is coupled to another mode following its transmission to distance (z), the power ratio of the new mode to the power of incident mode HE_{11} at incidence ($z=0$) is cross transmission power. An LPG power spectrum can be obtained by drawing a diagram of the relationship between these two parameters and the wavelength. We simplified the coupled-mode theoretical method in the previous section, and used the minimal mathematical formulae to provide the most complete and understandable physical concept introduction. Evidently, the traditional coupled-mode theory is not only a significant mathematical burden for novice learners of LPG, but its daunting difficulty is also dreaded by application-level designers. Obviously, for novice learners and application-level designers of LPG, the completion of the LPG design and analysis would invariably involve considering numerous mathematical equations, indirectly increasing the requirements and prerequisite domain knowledge for entering this field. This study employed a numerical technique that combines the finite element method (FEM) and eigenmode expansion method (EEM) in the LPG design and simulation. This study shows that by using this numerical technique, the design and analysis of LPG can be effortlessly accomplished without using any mathematical equations by novice learners and application-level designers. In addition, the extensive use of graphics may help novice learners and application-level designers visually understand the transmission of optical signals in LPG, which is otherwise unachievable through the traditional coupled-mode theory. This constitutes the contribution and novelty of the present study. To the best knowledge of the author, the significant and original findings reported in this study are not published elsewhere.

The traditional coupled-mode theory is based on the perturbation theory, which allows the input mode to interact with other guided modes during transmission to achieve a power exchange. As a well-established theory, the traditional coupled-mode theory has been extensively applied in various domains. The conversion of energy between modes is the core concept of the traditional coupled-mode theory. However, such a core value cannot be graphically manifested. Many of the 40–50 papers that the author has read thus far have adopted the traditional coupled-mode theory to conduct various component designs. However, none of these studies have demonstrated the phenomenon of power transmission in the component after completing component designs. By contrast, the present study represents the process of power conversion in graphical form, thus offering originality and contributions to this literature.

A crucial blind spot exists in the literature pertaining to the traditional coupled-mode theory. Specifically, the “AC” coupling coefficient is a key parameter for the entire traditional coupled-mode theory; in addition, it is a key element for power coupling, without which no power coupling could be generated between

different modes. Among numerous published works in which the traditional coupled-mode theory is applied, few have literally provided the calculation result of the "AC" coupling coefficient. The failure to provide a calculation result causes their research to be proven entirely erroneous. Conversely, this further highlights the value and significance of the present study. Using the proposed numerical method, novice learners and application-level designers may directly observe the transmission of optical signals in the LPG from the calculation results, which helps explain the generation of coupling effects through LPG. In summary, the core contribution of this study is in its simplicity and graphical representation. Furthermore, the method introduced in the present study may be widely applied to component designs that have a periodical structure, as opposed to the traditional coupled-mode theory that can only be applied to structures within a narrow and specific scope. In summary, compared to the LPG design methods proposed in other studies, the proposed approach provides a unique contribution in its simplicity and graphical representation.

The remaining content of this study is organized as follows: Section 2 contains a brief introduction to the finite element method (FEM). Regarding this numerical method, the decomposition resolution of the triangular element inevitably influences the correctness of the acquired mode. From a mathematical perspective, if all acquired modes are correct, the orthogonal values between the modes should be zero. Therefore, this study used a reverse-thinking method by initially determining an acceptable orthogonal value (10^{-4}), and then adjusting the decomposition resolution for simulation. In addition, tests may be performed at any time to confirm that the orthogonal value of the obtained modes is smaller than 10^{-4}.

Section 3 provides an introduction to theories related to the eigenmode expansion method. This section contains a detailed explanation of how the eigenmode expansion method facilitates the transmission of the guided mode in the LPG structure. In this section, we also discuss the main reason this method is substantially superior to the finite-difference time-domain (FDTD) method and beam propagation method. However, the numerical method proposed in this study also exhibited accuracy problems. The primary principle of optical wave transmission in the eigenmode expansion method centers on the Fourier series expansion. Even in a nonabsorbent medium, if an insufficient number of guided modes are used during the transmission process, the total power decreases as the transmission distance increases. Therefore, this study adopted a reverse-thinking method and experimented with using various numbers of guided modes for transmission to observe the dissipation of power during this process. Subsequently, the appropriate number of guided modes used in this study could be determined. In the actual design process, we verified the results by monitoring a relationship diagram of the power dissipation and transmission distance.

In Section 4, the content in Sections 2 and 3 are combined, and all LPG analyses and designs are conducted following a precise, simple, and complete design process. Additionally, we employ numerous graphics to present the simulation results, and use visualized and simplified methods to facilitate the formulated and abstracted learning process of coupled-mode theory.

In the final section, we summarize the numerical simulation method proposed in this study, and use the data obtained in Section 4 to verify that the proposed method can provide a visualized and simple simulation technique that can be applied to large periodic components, thereby reducing the required learning time and professional threshold for LPG research and application.

2. The finite element method

The finite element method is a numerical simulation method that has been widely used in various fields of engineering. Because the principles of the algorithm used in this method have been thoroughly explained in numerous studies [14], in this section, we only briefly introduce the main concepts of this method. Instead, we focused on how the FEM can be used to solve all existing guided modes in a fiber structure.

The finite element method is a numerical method used to solve partial differential equations (PDE) that satisfy boundary conditions. This method is based on the variational principle, domain decomposition, and interpolation function. The finite element method uses the variation principle (the variation algorithm) to transform the original problem (PDE with boundary conditions) into functional extreme value problems different from the original problem but with equivalent values. In other words, the same physical problem has two mathematical descriptions. That is, "boundary conditions + PDE = the functional for determining the minimum value." After determining the functional extreme value problem equivalent to the original problem, we applied the interpolation function and decomposed the domain we hoped to solve to convert the problem in which the functional solved for the minimum value into a set of multiple linear algebraic equations. We obtained the solution to the original problem by solving these linear algebraic equations. The algorithm of the finite element method comprises the following five steps:

A. Use the equivalent functional for solving the minimum value problem to replace the PDE with boundary conditions.
B. Divide the target solution domain into several sufficiently small segments that are often called elements, such as triangular elements and quadrilateral elements; the objects connecting elements are called nodes, and the unknown variables of the nodes are the target solutions.
C. The actual unknown function in each element is approximated by an appropriate interpolation function. The simplest interpolation function is the linear interpolation function. Thus, the polynomial function formed by nodes can be employed for approximation of the true function to be solved in each element. The coefficient of this polynomial is called a shape function
D. Integrate this polynomial into the functional to calculate the minimum value and obtain a set of simultaneous equations
E. Integrate the boundary conditions into the simultaneous equations, and use the Gaussian elimination method to solve the equations; subsequently obtain the solutions to all nodes in the target solution domain. After the solutions to the nodes are obtained, the true functions to be solved in each element can be approximated using the polynomial functions comprising nodes. Therefore, we can obtain all the unknown variables in the entire target solution geometric domain.

In this study, the triangular element method was employed to decompose the geometric area of the fiber X–Y plane, as shown in Fig. 2. The greater the decomposition resolution, the more accurate the calculation results become; however, the calculation amount significantly increases. Therefore, how to appropriately discretize the resolution area will inevitably become one of the core techniques of the FEM. As mentioned in the previous section, theoretically, all modes must be orthogonal regarding the relationship between the acquired modes and the decomposition resolution. The orthogonal values are expressed in the following equation:

$$\int_{A\infty} E_{t\nu} \times H_{t\mu} \cdot \hat{z}\, dA = \int_{A\infty} E_{t\mu} \times H_{t\nu} \cdot \hat{z}\, dA = 0 \quad \text{for } \nu \neq \mu \tag{6}$$

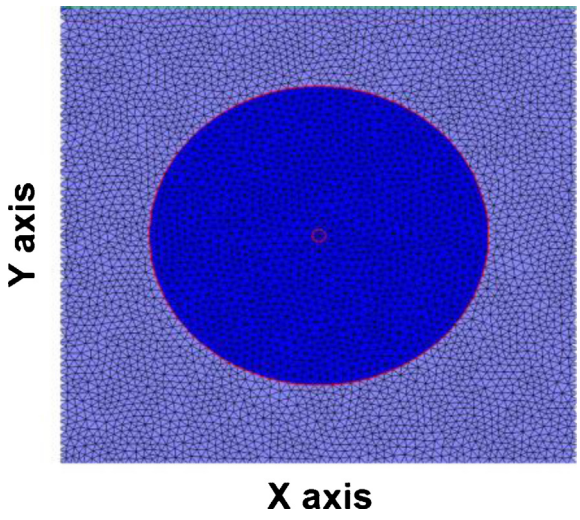

Fig. 2. A schematic diagram of using FEM to perform triangular element decomposition on the *X*–*Y* plane of an optical fiber.

However, regarding numerical simulations, problems such as an extremely large memory capacity and long mode solution time are inevitable. To accommodate the server's computational capacity, we reviewed the orthogonal values of the obtained modes to adjust the resolution of triangular decomposition appropriately. Unless otherwise indicated, all the decomposition resolutions in this study have orthogonal values that are smaller than 10^{-4}.

Following the completion of the decomposition process, all guided modes existing in the structure were resolved. The operating wavelength was $\lambda = 1550$ nm. Because a single-mode optical fiber was used, we obtained only one core mode, that is, HE_{11}, with an effective refractive index of n_{eff}^{core} ($n_2 < n_{eff}^{core} < n_1$), and a nearly infinite number of cladding modes, with an effective refractive index of $n_{eff}^{cladding}$ ($n_3 < n_{eff}^{cladding} < n_2$). Notably, fiber grating was uniformly distributed on the *X*–*Y* plane, indicating that when the core mode (HE_{11}) enters the LPG area, the couple-mode phenomenon only occurs between HE_{11} and the cladding modes of azimuthal order $l = 1$. Therefore, in this study, we focused on resolving and examining $l = 1$ cladding modes. The core mode (HE_{11}) was acquired after employing the FEM, and its two-dimensional (2D) and three-dimensional (3D) power distributions are shown in Figs. 3 and 4, with an effective refractive index of $n_{eff}^{core} = 1.451975$. Furthermore, the 2D and 3D power distributions of the cladding mode ($\nu = 1$) are shown in Figs. 5 and 6, with an effective refractive index of $n_{eff}^{\nu=1} = 1.449947$, and the 2D and 3D power distributions of the cladding mode ($\nu = 3$) are shown in Figs. 7 and 8, with an effective refractive index of $n_{eff}^{\nu=3} = 1.449769$. Finally, the 2D and 3D power distributions of the cladding mode ($\nu = 7$) are shown in Figs. 9 and 10, with an effective refractive index of $n_{eff}^{\nu=5} = 1.449055$, and the 2D and 3D power distributions of the cladding mode ($\nu = 11$) are shown in Figs. 11 and 12, with an effective refractive index of $n_{eff}^{\nu=21} = 1.447881$. We initially resolved 30 guided modes comprising one core mode (HE_{11}) and 29 cladding modes ($\nu = 1 - 29$; $l = 1$). We used the same naming convention commonly employed in fiber optics to name all of the guided modes obtained, excluding the core mode. We then numbered the 19 cladding modes based on their effective refractive index value, where the greater the n_{eff} value was, the smaller the ν value became. Therefore, based on the effective refractive index values, from highest to lowest, the 19 cladding modes were represented as $\nu = 1 - 29$. According to the descriptions mentioned previously, a higher order of the cladding mode indicates that its effective refractive index value approaches n_3, that is, the higher the order of the cladding mode, the larger the energy distribution range in the cladding layer. In other words, the higher order of the cladding mode suggests that its sensitivity to changes in the surrounding refractive index (n_3) is greater. Additionally, the calculation and test results of the orthogonal values between these 30 modes are shown in Fig. 13. The results indicate that besides each mode having a self-orthogonal value of 1, the orthogonal values between two different modes could satisfy the requirement of being less than 10^{-4}.

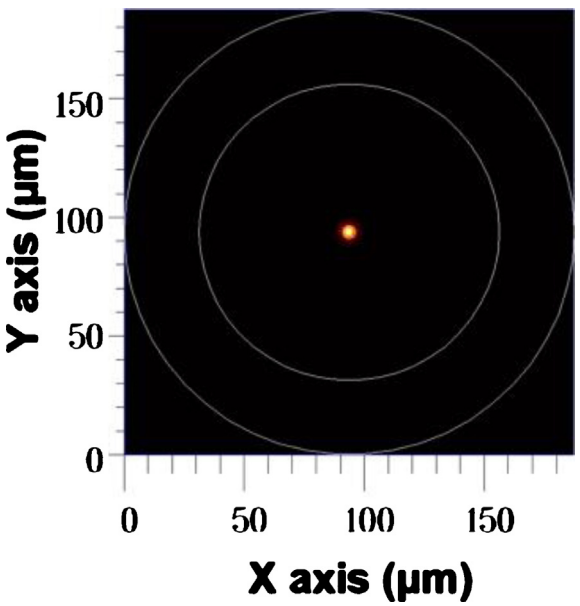

Fig. 3. The 2D power distribution of the core mode (HE_{11}), with an effective refractive index of $n_{eff}^{core} = 1.451975$.

3. The eigenmode expansion method

The primary objective of this method was to induce the guided mode to transmit power in the fiber structure. First, this method captured one segment object from the LPG periodic object and the length of the segment object is one period of the LPG periodic object, as shown in Fig. 14. The diagram clearly indicates that the LPG periodic object is composed of *N* segment objects. The length of each segment object represents one LPG period. Further cutting of each segment object produces mini objects called block objects

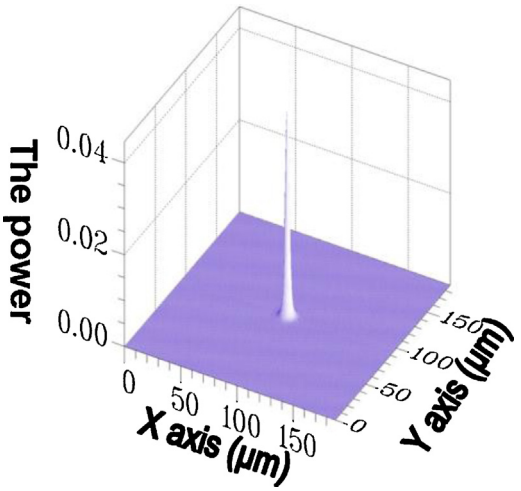

Fig. 4. The 3D power distribution of the core mode (HE_{11}), with an effective refractive index of $n_{eff}^{core} = 1.451975$.

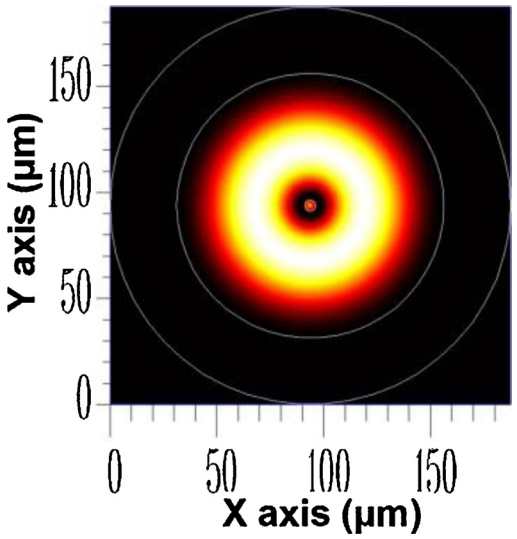

Fig. 5. The 2D power distribution of the cladding mode ($\nu=1$), with an effective refractive index of $n_{eff}^{\nu=1} = 1.449947$.

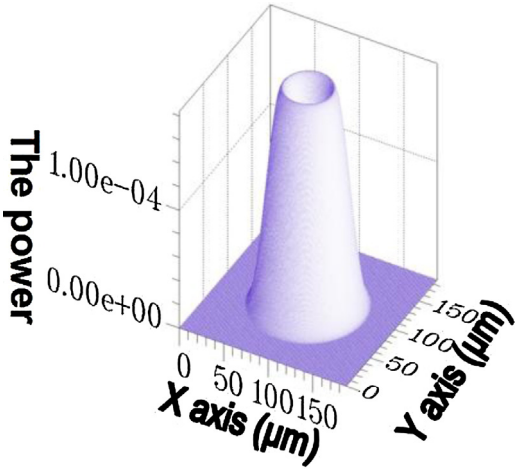

Fig. 6. The 3D power distribution of the cladding mode ($\nu=1$), with an effective refractive index of $n_{eff}^{\nu=1} = 1.449947$.

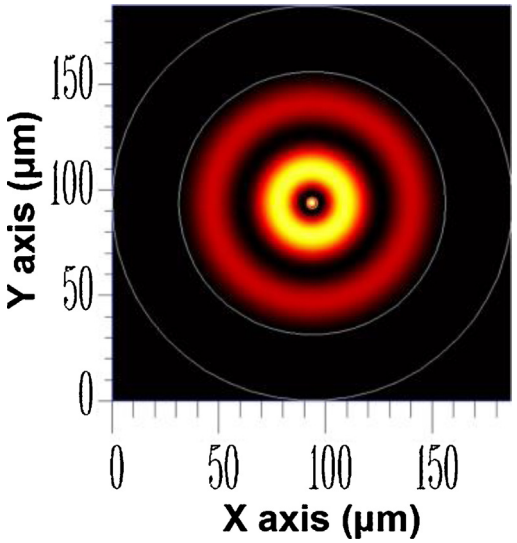

Fig. 7. The 2D power distribution of the cladding mode ($\nu=3$), with an effective refractive index of $n_{eff}^{\nu=3} = 1.449769$.

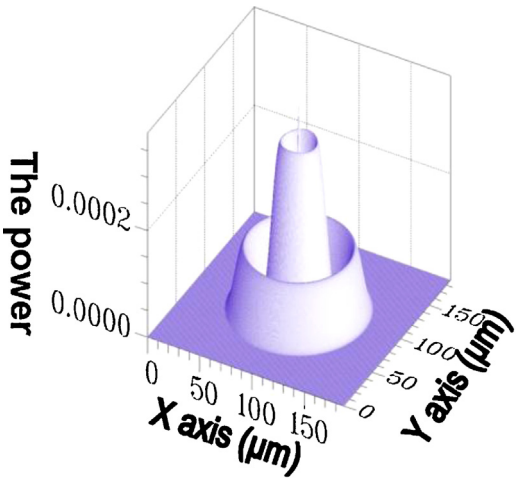

Fig. 8. The 3D power distribution of the cladding mode ($\nu=3$), with an effective refractive index of $n_{eff}^{\nu=3} = 1.449769$.

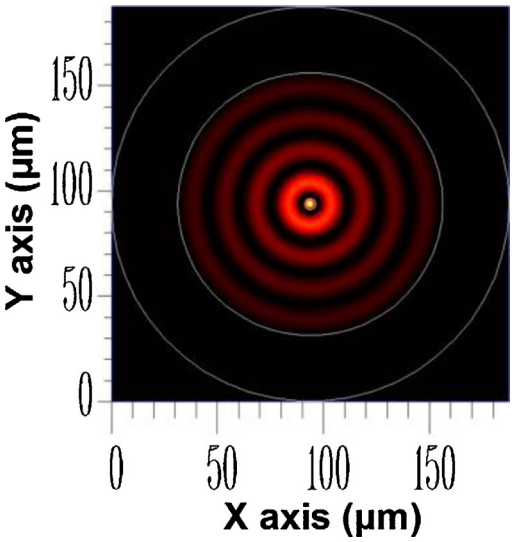

Fig. 9. The 2D power distribution of the cladding mode ($\nu=7$), with an effective refractive index of $n_{eff}^{\nu=7} = 1.449055$.

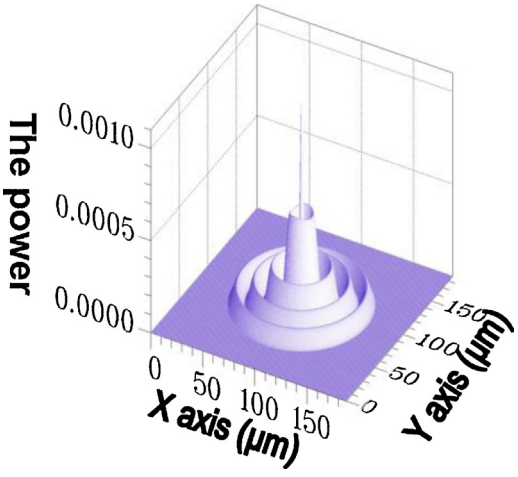

Fig. 10. The 3D power distribution of the cladding mode ($\nu=7$), with an effective refractive index of $n_{eff}^{\nu=7} = 1.449055$.

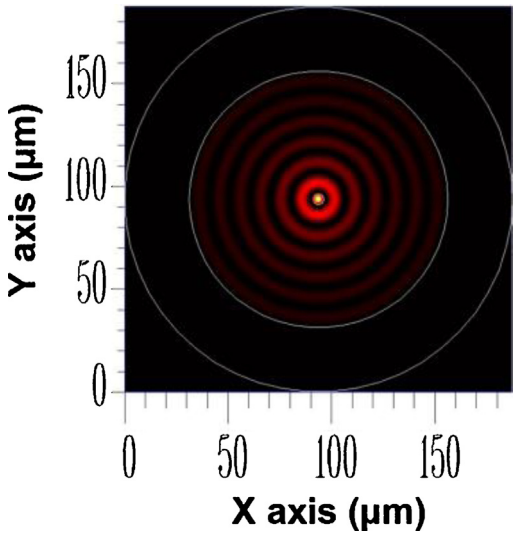

Fig. 11. The 2D power distribution of the cladding mode ($\nu = 11$), with an effective refractive index of $n_{eff}^{\nu=11} = 1.447881$.

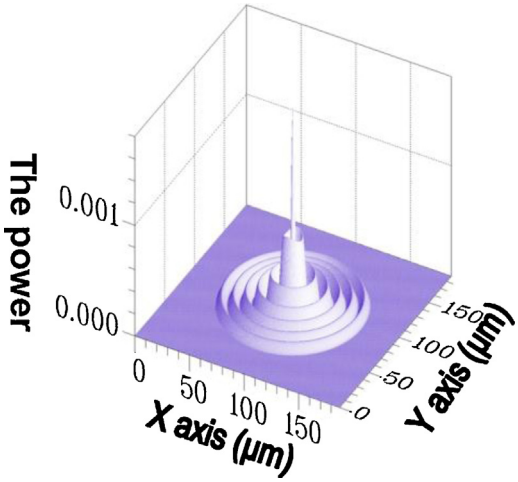

Fig. 12. The 3D power distribution of the cladding mode ($\nu = 11$), with an effective refractive index of $n_{eff}^{\nu=11} = 1.447881$.

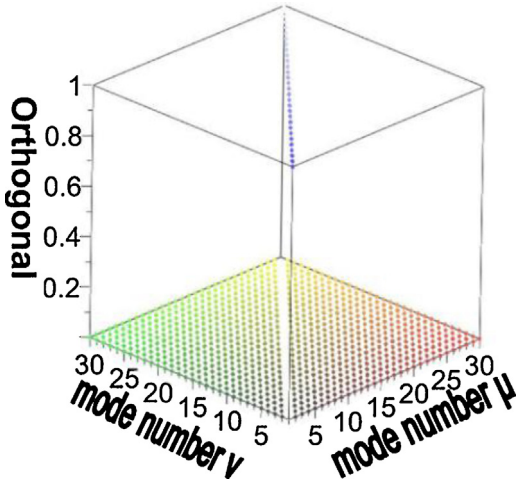

Fig. 13. Diagram of the relationships between the orthogonal values of the 30 modes.

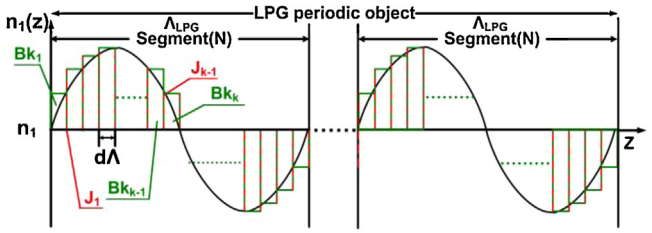

Fig. 14. Each cut block object in a segment object is considered a uniform waveguide with a fixed refractive index.

(Bk) with a length of $d\Lambda$. Each block object is considered a uniform LPG waveguide possessing a fixed refractive index value in the core layer. The contact surface between block object $k-1$ (Bk_{k-1}) and block object k (Bk_k) is called junction $k-1$ (J_{k-1}), which is presented in Segment (1) of Figs. 14 and 15. The diagram clearly shows that by employing the same cutting mechanism, the block objects obtained from cutting segment object (m) and segment object (n) are identical completely. In other words, under the same cutting procedure, completing the cutting computation for a segment object equates to completing the cutting computation for an entire LPG periodic object. In this study, we cut a segment object into 300 uniform block objects. The eigenmode expansion method targeted one segment object from the LPG periodic object and the segment was cutted into 300 uniform block objects ($N = 300$). In each block object, the guided modes that may exist were recalculated. Next, power conversions between block objects were performed using the Fourier series expansion method. The steps in this procedure can also be performed to complete the power transfers of the entire LPG [15–17].

This brief explanation provides an understanding of periodic components. The guided modes that can exist in each period of a periodic component are identical; therefore, when the finite element method is used to solve guided modes, it suffices to calculate only one period, as shown in Fig. 14. Thus, the calculation time and memory capacity consumed during component simulation is greatly reduced. Therefore, combining FEM and EEM is particularly suitable when designing components with periodic structures, such as the fiber-grating optical add-drop multiplexer, the long-period fiber-grating surface-plasmon-resonance sensor, the D-type long-period fiber-grating surface-plasmon-resonance sensor, and the crystal D-type long-period fiber-grating surface-plasmon-resonance sensor. Regarding the current calculation mechanism of the FDTD method, a 2–3-cm LPG under a $\lambda = 1550$ nm operating wavelength is massive; therefore, simulation and calculation are impossible. Even when using supercomputers to calculate a 2–3-cm LPG, the amount of time and memory required for the calculations is unimaginable. Additionally, the computation mechanism of the beam propagation method has an excessive number of restrictions and errors when used in multiple-reflection three-dimensional optical fiber structures. The preceding explanation clearly shows that the single period calculation is the main reason

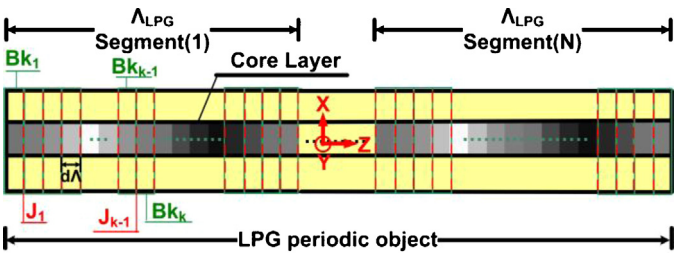

Fig. 15. Cutting schematic for the LPG periodic object.

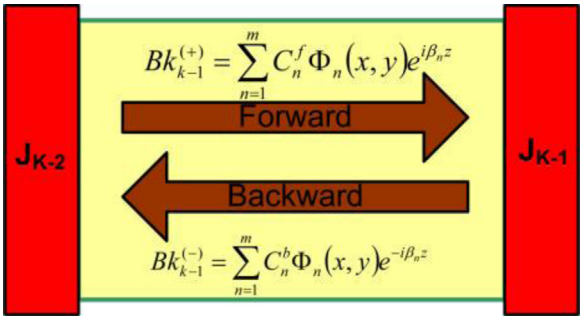

Fig. 16. Fourier series expansion for the forward and backward propagation modes.

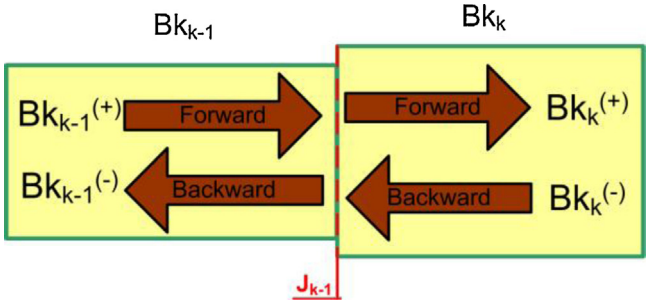

Fig. 17. The relationship between the field strength of the two adjacent uniform block objects Bk_{k-1} and Bk_k.

that the combination of FEM and EEM are significantly superior to FDTD and BPM.

Below we explain how the eigenmode expansion method is applied to LPG power propagation. Previous explanations have indicated that the LPG within a period is decomposed into several uniform waveguides. We hypothesized that the solution of the Maxwell equations in each uniform waveguide is equivalent to Eq. (7), where the mode content Φ_n and propagation constant β_n are eigenfunctions and eigenvalues obtained from the FEM.

$$E(x,y,z) = \Phi_n(x,y)\ \ e^{i\beta_n z} \tag{7}$$

By combining Eq. (7) with the Fourier series expansion concept, and adding the entire forward propagation mode $Bk_k^{(+)}$, as shown in Eq. (8), and the back propagation mode $Bk_k^{(-)}$, as shown in Eq. (9), obtained using the finite element method, where $m = 30$ was the guided mode amount, and C_n^f and C_n^b were the coefficients for each forward and backward mode field, as shown in Fig. 16, the electric and magnetic fields within the uniform block object Bk_{k-1} can be obtained, as shown in Eqs. (10) and (11).

$$Bk_k^{(+)} = \sum_{n=1}^{m} C_n^f \Phi_n(x,y) e^{i\beta_n z} \tag{8}$$

$$Bk_k^{(-)} = \sum_{n=1}^{m} C_n^b \Phi_n(x,y) e^{-i\beta_n z} \tag{9}$$

$$E(x,y,z) = \sum_{n=1}^{m} (C_n^f e^{i\beta_n z} + C_n^b e^{-i\beta_n z}) E_n(x,y) \tag{10}$$

$$H(x,y,z) = \sum_{n=1}^{m} (C_n^f e^{i\beta_n z} - C_n^b e^{-i\beta_n z}) H_n(x,y) \tag{11}$$

After the propagated electromagnetic fields for a uniform block object Bk_{k-1} are obtained, power must be precisely transferred from Block object Bk_{k-1} to Block object Bk_k. Here, we used the scattering matrix to transform the forward and backward power propagation of two adjacent block objects, as shown in Eq. (12). In Fig. 17, $Bk_{k-1}^{(+)}$, $Bk_k^{(+)}$ and $Bk_{k-1}^{(-)}$, $Bk_k^{(-)}$ were the total of the forward and backward propagation modes for the uniform block object Bk_{k-1} and the uniform block object Bk_k, and J_{k-1} was the scattering matrix of the adjacent block object junctions.

$$\begin{bmatrix} Bk_{k-1}^{(-)} \\ Bk_k^{(+)} \end{bmatrix} = J_{k-1} \begin{bmatrix} Bk_{k-1}^{(+)} \\ Bk_k^{(-)} \end{bmatrix} \tag{12}$$

To convert power between adjacent block objects, we employed the Fourier series expansion to obtain the unknown junction scattering matrix J_{k-1}. Finally, the coupling effects of LPG could be accurately conducted and completed by following the steps of this method. After considering detailed descriptions of the EEM, we can clearly determine that for periodic objects, only one segment object (that is, one period) is required during the cutting and mode-solving procedures. Then, by calculating each junction scattering matrix J_{k-1}, we can complete the simulation of the period object's modal transfer phenomenon. In summary, the ability to cut one single segment object and solve modes is the primary reason the EEM is superior to FDTD on calculation time and amount of memory used. In the traditional coupled-mode theory, the solution calculation of the guided modes occurred only at the beginning of the X–Y cross-section, and throughout the entire process of the optical signal passing through the LPG, the guided modes were never re-calculated. Therefore, the traditional coupled-mode theory emphasizes that the peak-induced index change (δn) of the LPG should not exceed 3×10^{-3} to avoid significant errors occurring in the traditional coupled-mode theory. Compared to the traditional coupled-mode theory, EEM employed in this study can detailed cut one segment into 300 uniform block objects and re-solve for the guided modes of each uniform block object. In other words, this method is not disadvantaged by requiring that the induced refractive index charge is not excessive. In addition, unless otherwise specified, all the induced refractive index changes in this study used $\delta n = 3.6 \times 10^{-3}$ as the guideline.

The detailed introduction to EEM indicates that the number of guided modes (m) in Eqs. (8)–(11) significantly influences the accuracy of this method. From a mathematical perspective, the Fourier series expansion must include all waveguide modes that exist in the structure; however, this is impossible from a numerical simulation perspective because of the excessive time and memory required to conduct the calculation. When the number of guided modes used is insufficient, power dissipation is inevitable when the modes pass the scattering matrices of the junctions of neighboring domains. Thus, we employed a reverse-thinking method in this study, and identified the minimum m value based on the condition that power dissipation should not exceed 10^{-4}. Fig. 18 shows the relationship between the transmission distance and power dissipation of the 30 guided modes used in EEM ($m = 30$). The results clearly indicate that 30 guided modes are sufficient for the LPG examined in this study. Therefore, unless otherwise specified, the criterion for all guided mode numbers was 30. Additionally, in the EEM algorithm method, the number of uniform block objects derived by slicing each segment influences the accuracy of the simulation results. Regarding the legitimacy of the algorithm method overall, an inspection standard was developed, that is, a specification indicating that the power loss must be less than 10^{-4}. If the power loss was not less than 10^{-4}, an appropriate amount for the number of modes solved and the number of block objects of each segment could be added to reduce the power loss. In addition, because the algorithm mechanism for the traditional coupled-mode theory differs from that of the proposed method in this study, a comparison of these two methods cannot be presented using common

Table 1
Comparison of the functions for CMT versus FEM and EEM.

Function algorithm	Use of mathematical equations	Presentation of mode excitation and power transmission diagrams	Acceptance level of novice learners and application-level designers	Presentation of spectral diagrams	Extensiveness of application
CMT	Widely varied and difficult	Excitation and transmission diagrams absent in the extant literature	Extremely low	Yes	Limited
FEM and EEM	Does not require any mathematical equations	Excitation and transmission diagrams can be easily presented using calculation results	Extremely high	Yes	Extensive

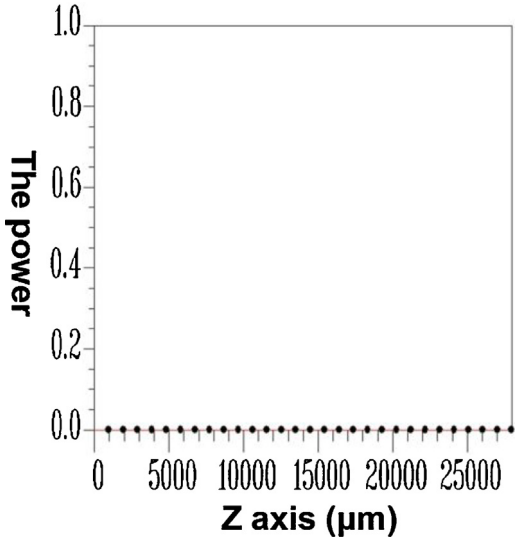

Fig. 18. The relationships between the transmission distance and power dissipation when employing 30 waveguides in the eigenmode expansion method.

parameters, figures, or graphs (aside from spectral diagrams). In other words, comparison of the two methods based on their spectral diagrams did not show significant differences. Thus, following the discussion on the two methods, a functional perspective was adopted to present the differences between these methods, as shown in Table 1.

4. LPG design and analysis

In this section, we introduce a precise, simple, and complete design process based on the numerical simulation methods examined in Sections 2 and 3, as shown in Fig. 19. All LPG analyses and designs were completed following this process. The geometric structure of the optical fiber used for the simulations in this section is shown in Fig. 20. $L_1 = 100\ \mu m$ and $L_3 = 100\ \mu m$ represent typical single-mode fibers, and $L_2 = N \times \Lambda\ (\mu m)$ represents a single-mode fiber with LPG. Combining FEM and EEM, we can rapidly scan the relationship of the transmission power and LPG period for the guided mode, as shown in Fig. 21. In other words, this diagram provides information regarding the period of LPG required for coupling the core mode to a specific co-directional propagation cladding mode.

Fig. 22 is a diagram of the relationship between the LPG period and the transmission power for the total coupling from the core mode to a co-propagating cladding mode ($\nu = 7$). Fig. 23 shows the relationship between the number of the LPG period and the transmission power for the total coupling from the core mode to a co-directional propagation cladding mode ($\nu = 7$). By simultaneously considering Figs. 22 and 23, we found that the core mode (HE_{11}) was completely coupled to the co-directional propagation cladding mode ($\nu = 7$) under period $\Lambda = 496.0408\ \mu m$ and a period number of $N = 56$. Based on these two parameters, we inputted the core mode (HE_{11}) from the left side of Fig. 20, and observed the power transmission of HE_{11} on the X–Z plane ($Y = 0$). The results are shown in Fig. 24. Under LPG interferences, the power of the core mode had completely coupled to the co-directional propagation cladding mode ($\nu = 7$) during the transmission process. To further verify the correctness of the mode coupling, we intercepted 2D and 3D power distribution diagrams from the output end (the right side) of Fig. 24, as shown in Figs. 25 and 26. Comparisons between Figs. 9 and 25 and between Figs. 10 and 26, showed that the figures had identical shapes, further verifying the accuracy of the method proposed in this study. In addition, to satisfy the criterion in Step 2 of the design process, the orthogonal values for this example were calculated and verified, as shown in Fig. 27. We observed that besides each mode having a self-orthogonal value of 1, the orthogonal values between two different modes could satisfy the requirement of being less than 10^{-4}. The transmission distance and power dissipation situations for this example also required calculation, as shown in Fig. 28. The dissipation satisfied the less than 10^{-4} criterion in Step 3 of the design process. In the traditional coupled-mode theory [12,13], numerous approximations and assumptions are used during equation derivation to obtain exact solutions. These approximations and assumptions include $\delta n \ll n_1$, neglecting the longitudinal coupling coefficient $K^z_{\nu-\mu}$, and the assumption that power coupling occurs only between two modes at any given time. Consequently, Eq. (2) was simplified into two-mode coupled-mode equations. Thus, Refs. [12,13] both indicated that the design wavelength λ_D and maximum wavelength λ_{max} exhibit inconsistency. By contrast, for the design process proposed by this study (Fig. 19), in Step 1, the operating wavelength is set as $\lambda_D = 1550$ nm, and all subsequent design steps are performed using this wavelength. The necessary LPG periods and the number of the LPG period were obtained in Step 4. The LPG parameters required to couple the core mode (HE_{11}) to the co-directional propagation cladding mode ($\nu = 7$) were $\Lambda = 496.0408\ \mu m$ and $N = 56$. Based on these parameters, we calculated the spectrum of the core mode, as shown in Fig. 29. From this diagram, we observed that the maximum transmission wavelength λ_{max} precisely matched the design of this study, that is, $\lambda_D = 1550$ nm.

In addition, we compared a spectrum diagram for the total coupling from the core mode to a co-directional propagation cladding mode ($\nu = 7$), as shown in Fig. 29, and a diagram (Fig. 30) of the relationship between the LPG period and the transmission power for the total coupling from the core mode to a co-directional propagation cladding mode ($\nu = 7$). We found that these two diagrams possessed a certain inverse relationship in the coupling period and wavelength. In other words, before spending a substantial amount of time on LPG spectrum calculations, we can glimpse at

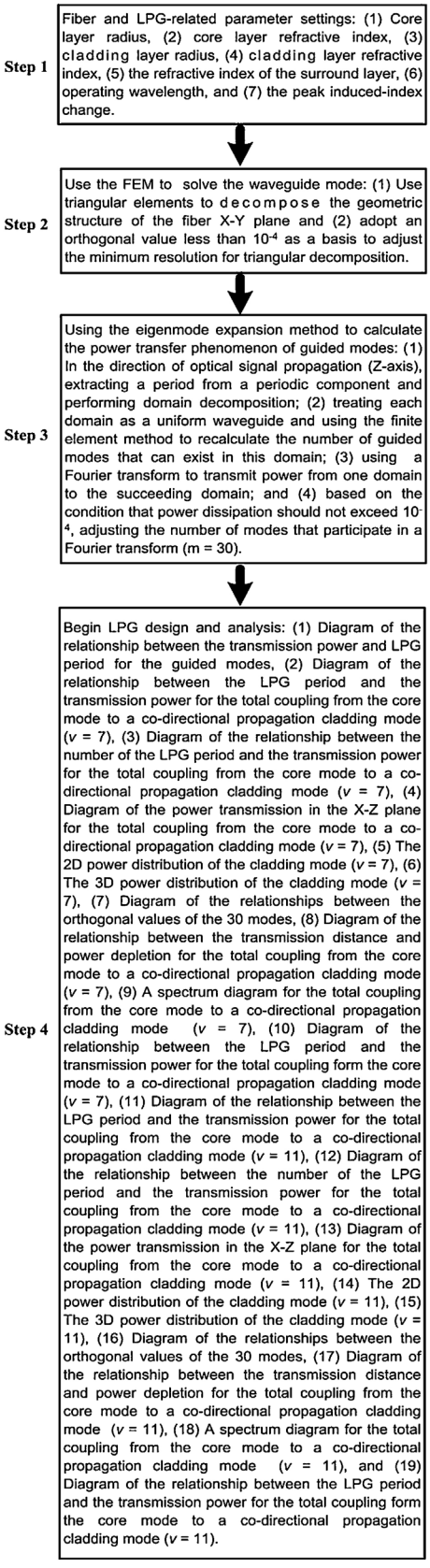

Fig. 19. LPG design and analysis process.

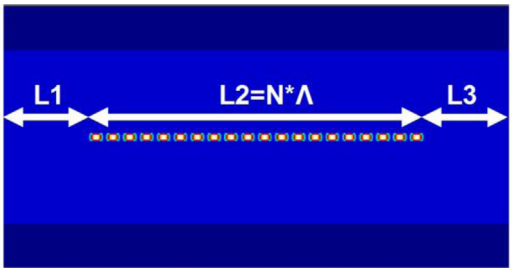

Fig. 20. The *X–Z* planar structure of the optical fiber used for numerical simulations.

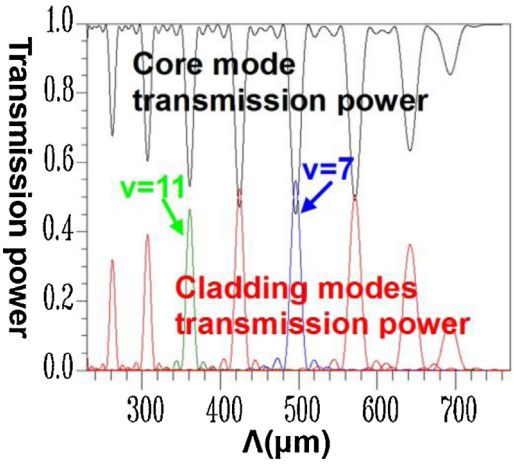

Fig. 21. Diagram of the relationship between the transmission power and LPG period for the guided modes.

the possible final spectrum in Fig. 30. This phenomenon can be explained using the following approximate, namely Eq. (13):

$$\lambda_D = \lambda_{\max} \cong (n_{eff}^{core} - n_{eff}^{cladding-\nu}) \cdot \Lambda. \quad (13)$$

In the spectrum, the LPG period (Λ) of Eq. (13) is a fixed constant. Therefore, the locations ($\lambda_D = \lambda_{\max}$) of various cladding modes (ν) in the spectrum are inverse (because of the minus sign in the equation) to the effective refractive index of each cladding mode ($n_{eff}^{cladding-\nu}$). In addition, the greater the cladding mode order (ν), the

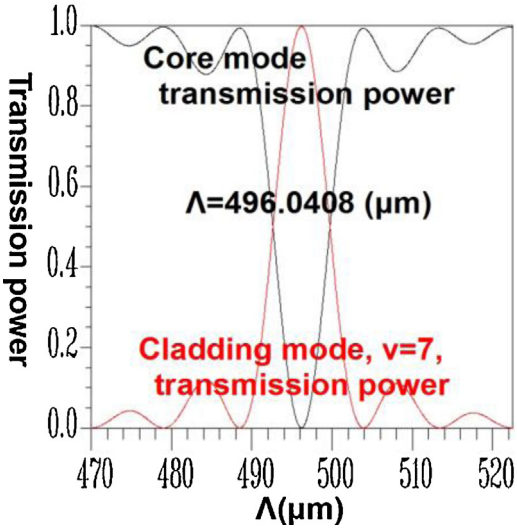

Fig. 22. Diagram of the relationship between the LPG period and the transmission power for the total coupling from the core mode to a co-directional propagation cladding mode (ν = 7).

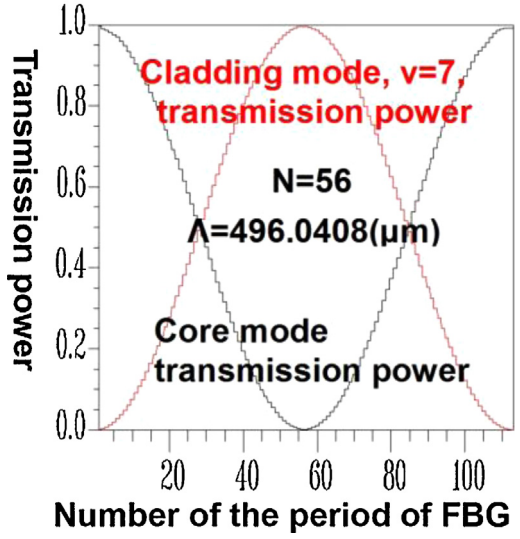

Fig. 23. Diagram of the relationship between the number of the LPG period and the transmission power for the total coupling from the core mode to a co-directional propagation cladding mode ($v = 7$).

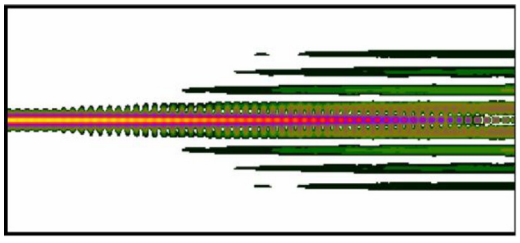

Fig. 24. Diagram of the power transmission in the X–Z plane for the total coupling from the core mode to a co-directional propagation cladding mode ($v = 7$).

smaller the effective refractive index. In other words, the coupled-mode ($\lambda_D = \lambda_{\max}$) locations range in the LPG spectrum from left to right as the mode order ascends. The LPG operating wavelength ($\lambda_D = \lambda_{\max}$) in the period scan is a fixed constant. However, the locations (Λ) of various cladding modes (v) in the period scan are proportional (because of the minus sign in the equation) to the effective refractive index ($n_{eff}^{cladding-v}$) of each cladding mode. In other words, the coupled-mode ($\lambda_D = \lambda_{\max}$) locations range in

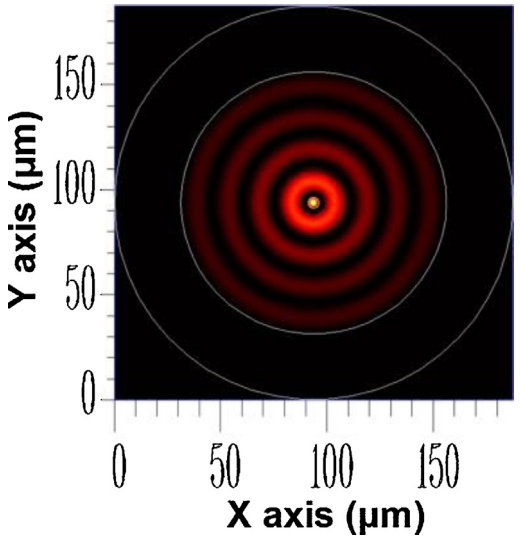

Fig. 25. The 2D power distribution of the cladding mode ($v = 7$).

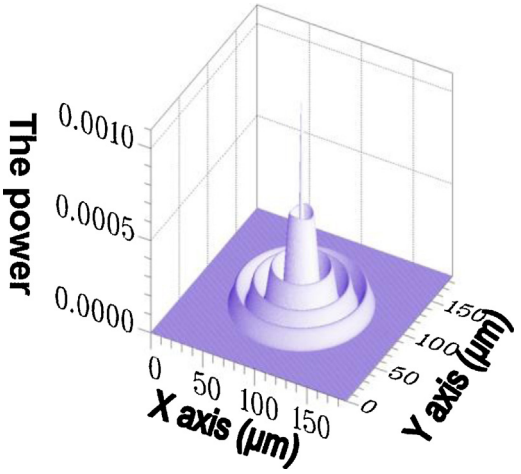

Fig. 26. The 3D power distribution of the cladding mode ($v = 7$).

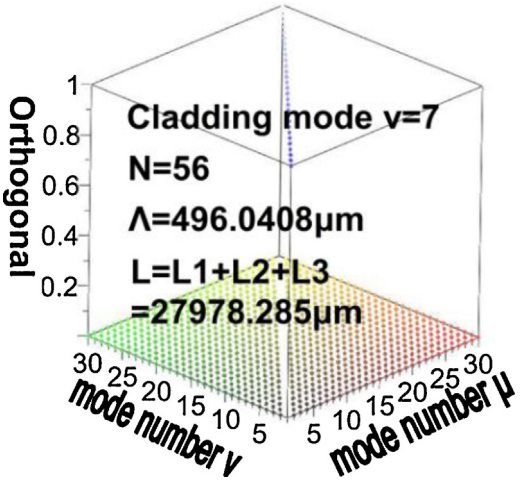

Fig. 27. Diagram of the relationships between the orthogonal values of the 30 modes.

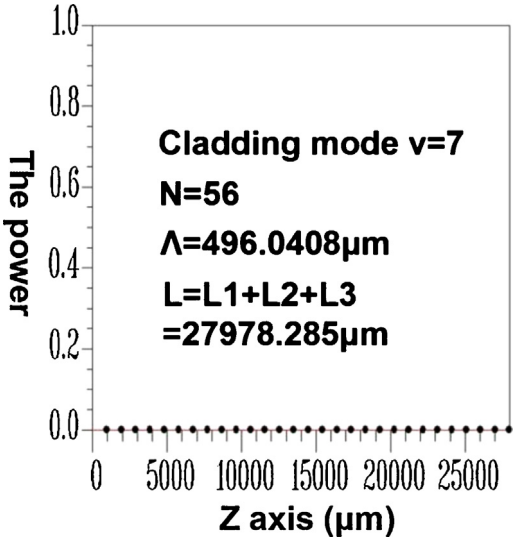

Fig. 28. Diagram of the relationship between the transmission distance and power dissipation for the total coupling from the core mode to a co-directional propagation cladding mode ($v = 7$).

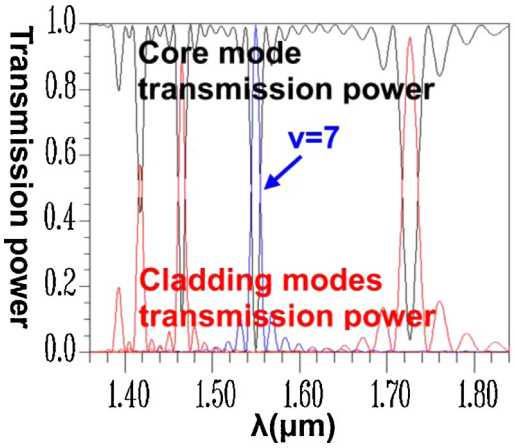

Fig. 29. A spectrum diagram for the total coupling from the core mode to a co-directional propagation cladding mode ($\nu = 7$).

the period scan from right to left as the mode order ascends. This clearly explains why the locations of all coupled-modes in the LPG spectrum and period scan exhibit an inversed phenomenon. In a separate example, we developed designs for the coupling phenomenon of the core mode (HE_{11}) and co-directional propagation cladding mode ($\nu = 11$), and adopted identical analysis techniques; the results are shown in Fig. 31.

Specifically, Fig. 31 shows a diagram of the relationship between the LPG period and the transmission power for the total coupling from the core mode to a co-directional propagation cladding mode ($\nu = 11$). Fig. 32 is a diagram of the relationship between the number of the LPG period and the transmission power for the total coupling from the core mode to a co-directional propagation cladding mode ($\nu = 11$). The combination of Figs. 31 and 32 indicates that the core mode (HE_{11}) was completely coupled to the co-directional propagation cladding mode ($\nu = 11$) when the period $\Lambda = 360.9107\,\mu m$ and the number of periods was $N = 63$. Similarly, we referenced the two parameters previously mentioned, and inputted the core mode (HE_{11}) into the left side of Fig. 20 to observe the power transmission of HE_{11} on the X–Z plane ($Y = 0$); the results are shown in Fig. 33. The power of the core mode was completely coupled to the co-directional propagation cladding mode ($\nu = 11$) during the transmission process. In addition, to verify the correctness of the coupled-mode, we intercepted 2D and 3D power distribution diagrams from the output end (the right side) of Fig. 33, as

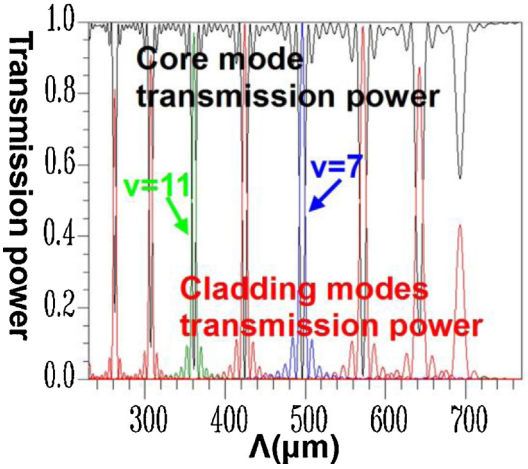

Fig. 30. Diagram of the relationship between the LPG period and the transmission power for the total coupling from the core mode to a co-directional propagation cladding mode ($\nu = 7$).

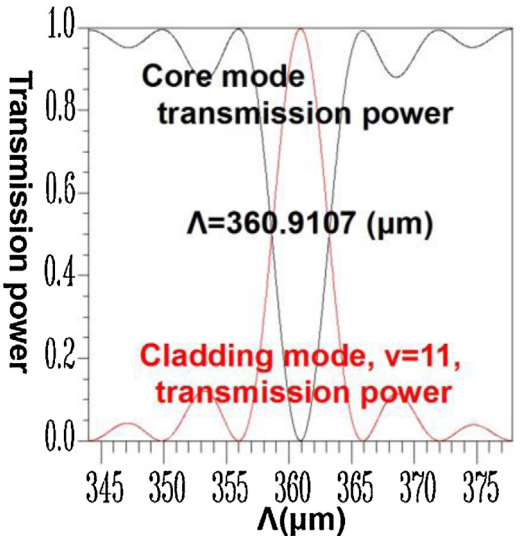

Fig. 31. Diagram of the relationship between the LPG period and the transmission power for the total coupling from the core mode to a co-directional propagation cladding mode ($\nu = 11$).

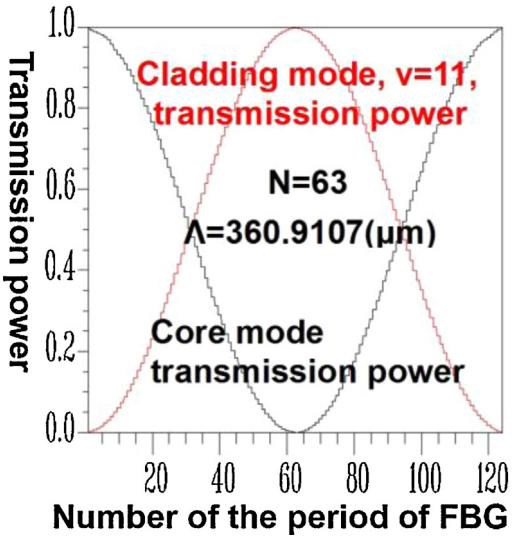

Fig. 32. Diagram of the relationship between the number of the LPG period and the transmission power for the total coupling from the core mode to a co-directional propagation cladding mode ($\nu = 11$).

shown in Figs. 34 and 35. The identicalness found when comparing Figs. 11 and 34 and Figs. 12 and 35 verify the correctness of the methods proposed in this study. In addition, to satisfy the design process criterion in Step 2, the orthogonal values of this example were calculated and verified, as shown in Fig. 36. We observed

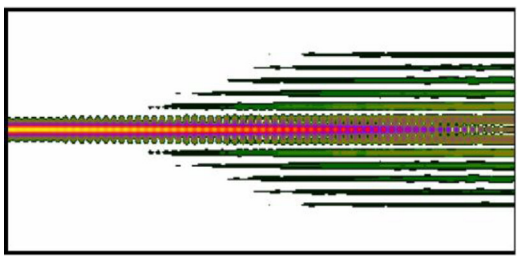

Fig. 33. Diagram of the power transmission in the X–Z plane for the total coupling from the core mode to a co-directional propagation cladding mode ($\nu = 11$).

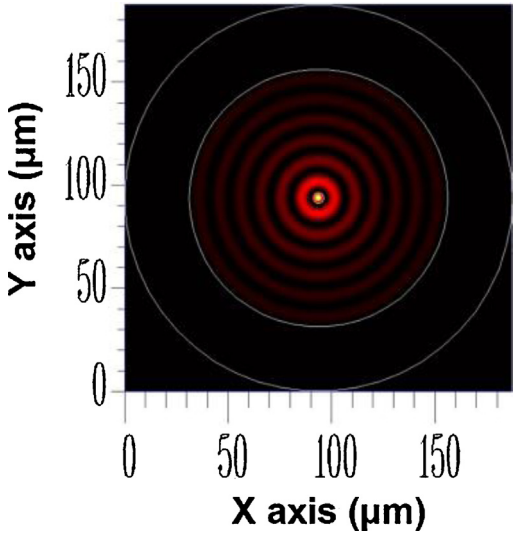

Fig. 34. The 2D power distribution of the cladding mode ($\nu = 11$).

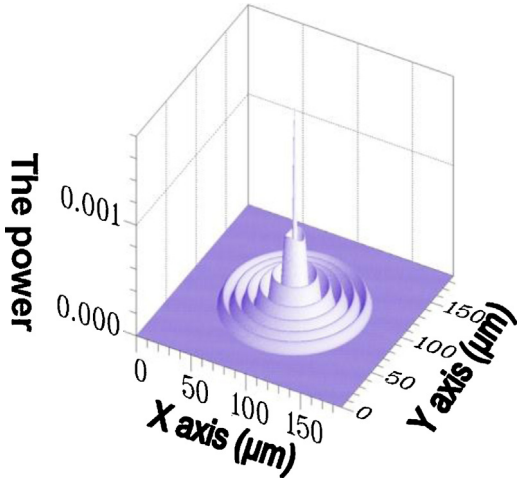

Fig. 35. The 3D power distribution of the cladding mode ($\nu = 11$).

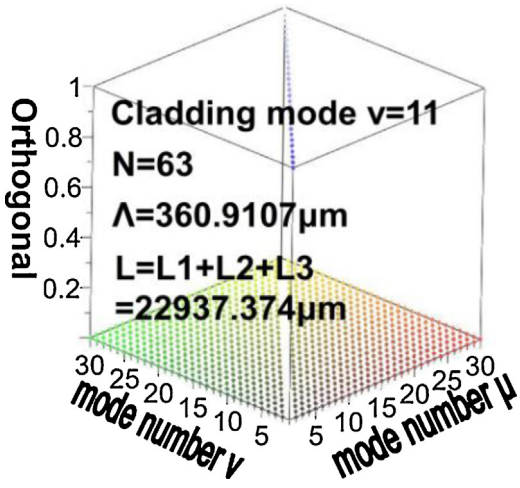

Fig. 36. Diagram of the relationships between the orthogonal values of the 30 modes.

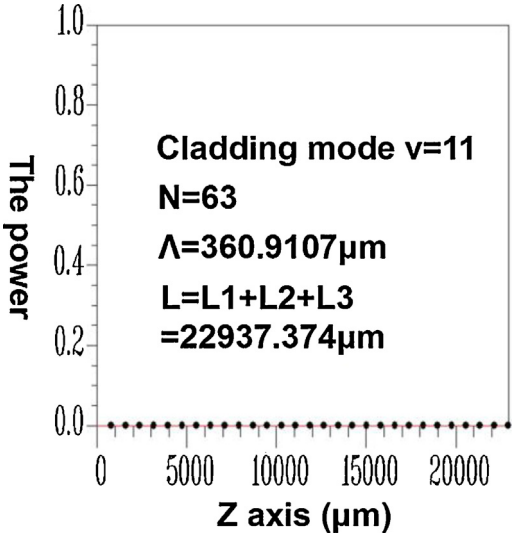

Fig. 37. Diagram of the relationship between the transmission distance and power dissipation for the total coupling from the core mode to a co-directional propagation cladding mode ($\nu = 11$).

that besides each mode having a self-orthogonal value of 1, the orthogonal values between two different modes could satisfy the requirement of being less than 10^{-4}. The transmission distance and power dissipation situations of this example also required testing. As shown in Fig. 37, the dissipation satisfied the less than 10^{-4} design process criterion of Step 3.

The LPG parameters required to couple the core mode (HE_{11}) to the co-directional propagation cladding mode ($\nu = 11$) were $\Lambda = 360.9107\,\mu m$ and $N = 63$. Based on these parameters, we calculated the spectrum of the core mode, as shown in Fig. 38. Significantly, the maximum transmission wavelength λ_{max} also matched our original designed wavelength of $\lambda_D = 1550$ nm. Furthermore, by comparing the spectrum diagram for the total coupling from the core mode to a co-directional propagation cladding mode ($\nu = 11$; Fig. 38) and the diagram of the relationship between the LPG period and the transmission power for the total coupling from the core mode to a co-directional propagation cladding mode ($\nu = 11$; Fig. 39), we found that these two diagrams possessed a certain inverse relationship in the coupling period and wavelength. In other words, these results verify that before spending a substantial amount of time on LPG spectrum calculations, we can see the possible final spectrum in Fig. 39.

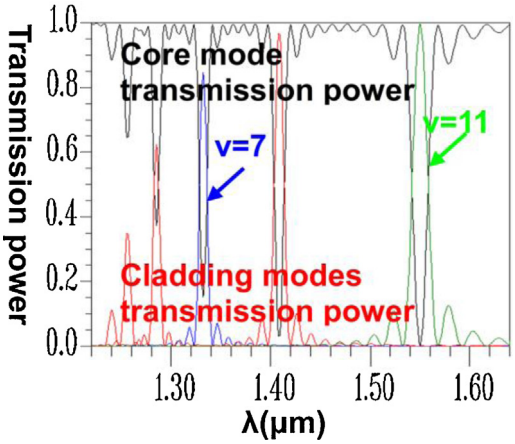

Fig. 38. A spectrum diagram for the total coupling from the core mode to a co-directional propagation cladding mode ($\nu = 11$).

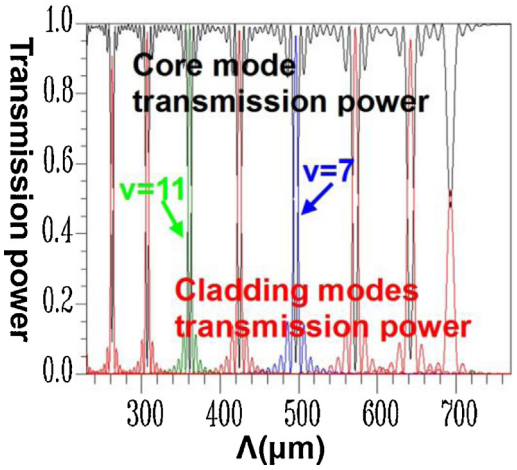

Fig. 39. Diagram of the relationship between the LPG period and the transmission power for the total coupling from the core mode to a co-directional propagation cladding mode ($v = 11$).

5. Conclusion

This study combined the FEM and the eigenmode expansion method with a precise, simple, and complete design process, and proposed a visualized, graphical, and simplified numerical simulation method to complete all LPG designs and analyses. Regarding 2–3 cm LPGs, no current numerical simulation methods can be employed for 3D analyses and design. In Section 3, we explained why the eigenmode expansion method can complete a significant amount of LPG analyses and designs using less memory and time. Section 3 demonstrated the distinctiveness and uniqueness of this study by presenting the interception, re-calculation, and solving for a single period component. In Section 4, we described the core techniques proposed in this study. Based on the numerous precise graphical results obtained in the design process, our objective was to assist LPG novices or application designers in employing graphical methods to facilitate their learning of the traditional coupled-mode theory upon entering the LPG field, and to reduce direct contact with formulized and abstract mathematical models. Significantly, compared to traditional coupled-mode theories, the maximum transmission wavelength λ_{max} of the LPG product completed using the design process described in Section 4 satisfies the design criterion λ_D. Additionally, a comparison of the scan of the FBG period and the spectrum of the final design indicated a certain inverse relationship between these two in the coupling period and wavelength. Therefore, before spending a substantial amount of time on FBG spectrum calculations, a possible final spectrum can be observed from a scan of the FBG period. In addition, power dissipation conditions and the mode orthogonal value were calculated and verified in both examples to ensure the compliance of the design procedure criterion. The primary objective of this study was to develop a numerical technique is precise, simple, and graphical as a supplement for traditional couple-mode theory, and further reduce the difficulty and fear of learning LPG.

Acknowledgment

The author gratefully acknowledges the support provided for this study by the National Science Council (NSC101-2622-E-007-CC3) of Taiwan.

References

[1] A.M. Vengsarkar, P.J. Lemaire, J.B. Judkins, V. Bhatia, T. Erdogan, J.E. Sipe, Long-period fiber gratings as band-rejection filters, Journal of Lightwave Technology 14 (1996) 58–65.
[2] A.M. Vengsarkar, J.R. Pedrazzani, J.B. Judkins, P.J. lemaire, Long-period fiber-gratingbased gain equalizers, Optics Letters 21 (1996) 336–338.
[3] D. Stegall, T. Erdogan, Dispersion control with use of long-period fiber gratings, Journal of the Optical Society of America A Optics and Image Science 17 (2000) 304–312.
[4] B. Judkins, A.M. Vengsarkar, Optical fiber long-period grating sensors, Optics Letters 21 (1996) 692–694.
[5] J.A. Besley, T. Wang, L. Reekie, Fiber cladding mode sensitivity characterization for long-period gratings, Journal of Lightwave Technology 21 (2003) 848–853.
[6] H.J. Patrick, A.D. Kersey, F. Bucholtz, Analysis of the response of long period fiber gratings to the external index of refraction, Journal of Lightwave Technology 16 (1998) 1606–1612.
[7] R. Falciai, A.G. Mignani, A. Vannini, Long period gratings as solution concentration sensors, Sensors and Actuators B 74 (2001) 74–77.
[8] Y.J. He, Y.L. Lo, J.F. Huang, Bandwidth analysis of long-period fiber grating for high order cladding mode and its application to optical add-drop multiplexer, Optical Engineering 45 (12 (8)) (2006) 125001.
[9] W.H. Loh, F.Q. Zhou, J.J. Pan, Novel designs for sampled grating based multiplexers demultiplexers, Optics Letters 24 (November) (1999) 1457–1459.
[10] Y.J. He, Y.L. Lo, J.F. Huang, Optical-fiber surface-plasmon-resonance sensor employing long-period fiber grating in multiplexing, Journal of the Optical Society of America B 23 (2006) 801–811.
[11] Ó. Esteban, R. Alonso, M.C. Navarrete, A. González-Cano, Surface plasmon excitation in fiber-optical sensors: a novel theoretical approach, Journal of Lightwave Technology 20 (2002) 448–453.
[12] T. Erdogan, Cladding-mode resonances in short and long period fiber grating filters, Journal of the Optical Society of America A 14 (1997) 1760–1773.
[13] T. Erdogan, Fiber grating spectra, Journal of Lightwave Technology 15 (1997) 1277–1294.
[14] D. Sun, et al., Spurious modes in finite-element methods, IEEE Antennas and Propagation Magazine 37 (12) (1995).
[15] C.H. Herry, Y. Shani, Analysis of mode propagation in optical waveguide devices by fourier expansion, IEEE Journal Quantum Electron 27 (1991) 523–530.
[16] G. Sztefka, H.P. Nolting, Bidirectional eigenmode propagation for large refractive index steps, IEEE Photonics Technology Letters 5 (1993) 554–557.
[17] D.F.G. Gallagher, T.P. Felici, Emgenmode expansion methods for simulation of optical propagation in photonics-Pros and cons, in: Proceedings of the Integratied Optics: Devices Materials and Technologies VII, SPIE 4987, 2003, pp. 69–82.

Biography

Yue Jing He received his MS degree in the Department of Communication Engineering from National Chiao-Tung University, Hsinchu, Taiwan, in 2000, and PhD degree in the Department of Electrical Engineering from National Cheng Kung University, Tainan, Taiwan, in 2006. After graduation, he has been a member of the faculty of the Electronic Engineering Department, National Chin-Yi University of Technology, Taichung, Taiwan, since 2008. His research interests are in the areas of the component design in optical fiber communication and in surface plasmon resonance sensor.